Journal of Alloys and Compounds 489 (2010) 152–156

Contents lists available at ScienceDirect

Journal of Alloys and Compounds

journal homepage: www.elsevier.com/locate/jallcom

Synthesis, structure, and magnetic property of hexagonal perovskite $Ba_5Sn_{1.1}Mn_{3.9}O_{15}$

Congling Yin[a], Guobao Li[a,*], Tounan Jin[b], Julian Tao[c], James W. Richardson[c], Chun-K. Loong[c], Fuhui Liao[a], Jianhua Lin[a,*]

[a] Beijing National Laboratory for Molecular Sciences, State Key Laboratory of Rare Earth Materials Chemistry and Applications, College of Chemistry and Molecular Engineering, Peking University, Beijing 100871, PR China
[b] College of Material Science and Engineering, Beijing University of Technology, Beijing 100022, PR China
[c] Intense Pulse Neutron Source Division, Argonne National Laboratory, Argonne, IL 60439, USA

ARTICLE INFO

Article history:
Received 4 June 2009
Received in revised form 8 September 2009
Accepted 9 September 2009
Available online 16 September 2009

Keywords:
Solid-state reaction
Crystal structure
Hexagonal perovskite
Barium tin manganese oxide
Magnetic property

ABSTRACT

A new compound $Ba_5Sn_{1.1}Mn_{3.9}O_{15}$ has been synthesized at 1300 °C by solid-state reaction. The structure was characterized by X-ray, electron and neutron diffraction methods. $Ba_5Sn_{1.1}Mn_{3.9}O_{15}$ crystallizes in hexagonal space group $P6_3/mmc$ with $a = 5.717$ Å and $c = 23.534$ Å. The magnetic measurement reveals that $Ba_5Sn_{1.1}Mn_{3.9}O_{15}$ has a spin glass transition at 7 K.

1. Introduction

Considerable interest has been focused on hexagonal perovskite $BaMnO_{3-\delta}$ system because of their rich structure chemistry [1–7]. A series of polytypes (2H → 15R → 8H → 6H → 10H → 4H) is found in reduced $BaMnO_{3-\delta}$ as the oxygen vacancy concentration y increases [4,5] (this notation shows the number of close-packed layers in the repeat sequence and the lattice symmetry as H = hexagonal, R = rhombohedral). New hexagonal perovskite polytypes are generated when Mn is substituted by different cations. Several doped $BaMnO_3$ systems including $Ba_{1-x}Sr_xMnO_{3-\delta}$ [5,8], $BaTi_xMn_{1-x}O_3$ [9], $BaCa_xMn_{1-x}O_{3-\delta}$ [10,11], $BaIr_xMn_{1-x}O_{3-\delta}$ [12], $BaLn_xMn_{1-x}O_{3-\delta}$ (Ln = rare earth element) [13–17], $BaIn_xMn_{1-x}O_{3-\delta}$ [18,19], $BaCo_xMn_{1-x}O_{3-\delta}$ [20,21], $BaRu_xMn_{1-x}O_3$ [22] and $BaFe_xMn_{1-x}O_{3-\delta}$ [23] have been explored. Among them, two B-cation ordered hexagonal perovskite structure are found with a formula $Ba_{n+1}XMn_nO_{3n-\delta}$ ($n = 2$, 3), which contains one layer of corner-sharing XO_6 octahedron and n layers of face-sharing MnO_6 octahedra [13–16,19]. Recently a new compound with $n = 4$ in this series, 10H-polytype compound $Ba_5In_{0.93}Mn_4O_{14.40}$ [18], was reported. Many efforts have been paid to synthesize other iso-structural compounds by replacing Indium ion with other metal ion. We found a narrow solid solution $B_5Sn_{1+x}Mn_{4-x}O_{15}$ in Sn-doped $BaMnO_3$ system. Here, the synthesis, structural characterization and magnetic properties of a typical sample $Ba_5Sn_{1.1}Mn_{3.9}O_{15}$, were reported.

2. Experimental

$Ba_5Sn_{1.1}Mn_{3.9}O_{15}$ was synthesized via high temperature solid-state reaction. The stoichiometric starting materials of $BaCO_3$ (A.R.), MnO_2 (A.R.), and SnO_2 (A.R.) were mixed in an agate mortar and pestle, and heated in an alumina crucible at 1000 °C for 10 h. Then, the sample was reground, pressed into pellets (20 ton/cm^2) and heated at 1300 °C for 30 h with several intermediate pressing and grinding steps and furnace-cooled each step.

The phase purity of the sample was checked by powder X-ray diffraction on a Rigaku D/Max-2000 diffractometer with graphite monochromatized Cu K_α radiation at 40 kV, 100 mA. Data were collected in the range of 6–120° with step scanning mode for Rietveld refinement carried out with GSAS program [24]. The neutron diffraction data were collected at different temperatures on the Special Environment Powder Diffractometer at the Intense Pulsed Neutron Source, Argonne National Laboratory. Selected-area electron diffraction (SAED) and convergent-beam electron diffraction (CBED) were carried out on Tecnai G^2 F30 with an accelerating voltage of 300 kV. The magnetic properties were investigated with a Quantum Design MPMS-SS superconducting quantum interference device (SQUID) magnetometer. Data were recorded in a 1000 Oe field while warming the sample from 2 to 300 K, following field cooling (FC).

* Corresponding authors. Tel.: +86 10 62750342; fax: +86 10 62753541.
E-mail addresses: liguobao@pku.edu.cn (G. Li), jhlin@pku.edu.cn (J. Lin).

0925-8388/$ – see front matter © 2009 Elsevier B.V. All rights reserved.
doi:10.1016/j.jallcom.2009.09.037

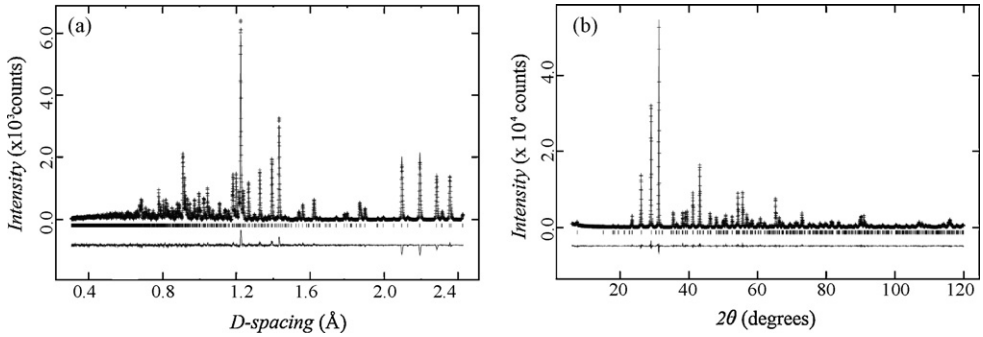

Fig. 1. Experimental, calculated, and differential diffraction pattern collected at room temperature of $Ba_5Sn_{1.1}Mn_{3.9}O_{15}$, (a) neutron and (b) X-ray.

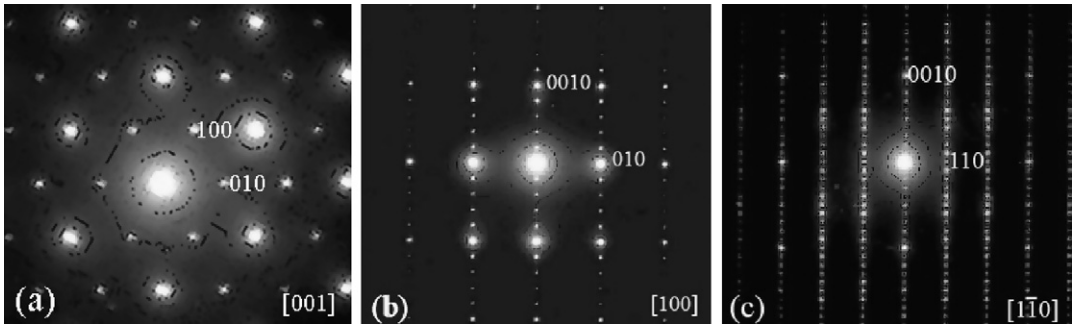

Fig. 2. SAED pattern of $Ba_5Sn_{1.1}Mn_{3.9}O_{15}$ along three projections: (a) [0 0 1], (b) [1 0 0], and (c) [1 $\bar{1}$ 0]. No superstructure spot can be observed.

3. Results and discussion

3.1. Crystal structure

The XRD pattern of $Ba_5Sn_{1.1}Mn_{3.9}O_{15}$ is plotted in Fig. 1b, which is similar to that of 10H $Ba_5In_{0.93}Mn_4O_{14.40}$ [18]. This suggests that $Ba_5Sn_{1.1}Mn_{3.9}O_{15}$ may adopt a 10H perovskite structure. The XRD pattern can be indexed [25] to a hexagonal cell with $a = 5.717$ Å and $c = 23.534$ Å. The systematic absence [26] of the reflections indicated the possible space groups, $P6_3/mmc$, $P\bar{6}2c$, $P6_3mc$, $P\bar{3}1c$ or $P31c$. Selected-area electron diffraction (SAED) was employed for further investigation. The SAED patterns along the most relevant zone axes [0 0 1], [1 0 0], [1 $\bar{1}$ 0], are shown in Fig. 2a–c, respectively. No superstructure reflection occurs and all the reflections in these patterns confirm the above indexing results. The systematic absence of the reflections was observed as $hh\overline{2h}l : l = 2n + 1$, which agrees well with the above space groups. All the spots are visible in Fig. 2c due to second diffraction.

Convergent-beam electron diffraction (CBED) is an effective tool to probe the crystal symmetry along certain projection. The CBED patterns along three relevant zone axes [0 0 1], [$\bar{1}$ 1 0], [$\bar{5}$ 4 0], are shown in Fig. 3a–c, respectively. The whole pattern symmetries are 6*mm* in [0 0 1], 2*mm* in [$\bar{1}$ 1 0] and *m* in [$\bar{5}$ 4 0], respectively. Only the space group $P6_3/mmc$ matches such whole pattern symmetry. So the space group $P6_3/mmc$ was chosen in the further Rietveld refinement.

The structure refinement was carried out with GSAS simultaneously on XRD and neutron diffraction data. Structural refinement adopted a 10H-$Ba_5In_{0.93}Mn_4O_{14.40}$ perovskite, which has the corner-sharing octahedral site M1 and the face-sharing octahedral sites M2 and M3 for B-site atoms, as shown in Fig. 4. In the first refinement step, the occupancy of Sn and Mn were refined at M1, M2 and Mn3 site with the sum of each site subject to unit. Minus Sn occupancy was found at M3 site, thus Mn occupancy at M3 site was set as unit. The occupancies of Sn and Mn were refined at M1 and M2 sites with Sn/Mn ratio subject to initial stoichiometry. In the second step, oxygen vacancy was refined. No oxygen vacancy was found within the refinement error. Thus the oxygen occupancies were subject to unit. The final refinement gave out a good fitting, shown in Fig. 1 for the XRD and neutron diffraction data.

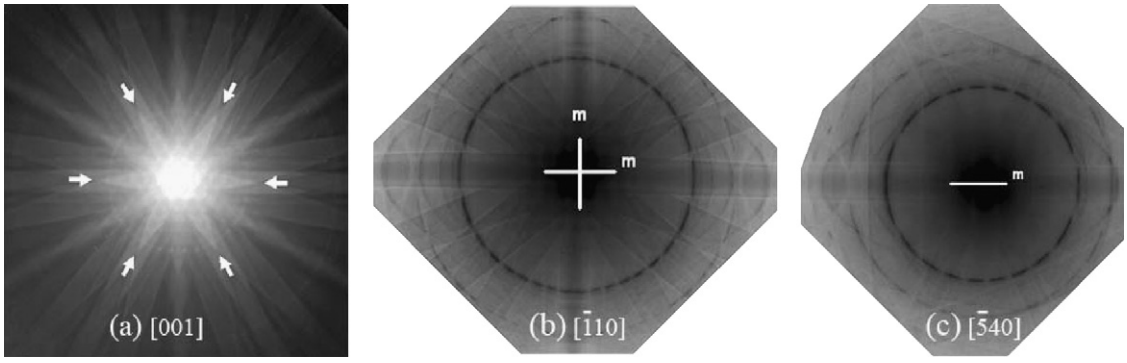

Fig. 3. CBED patterns of $Ba_5Sn_{1.1}Mn_{3.9}O_{15}$ along (a) [0 0 1], (b) [$\bar{1}$ 1 0] and (c) [$\bar{5}$ 4 0], whose whole pattern symmetry is 6*mm*, 2*mm* and *m*, respectively.

Table 1
Rietveld refinement results of $Ba_5Sn_{1.1}Mn_{3.9}O_{15}$.

Atom	Site	*x*, *y*, *z*	Occup.	100*xU*/Å^2	BVS
Ba1	2d	2/3, 1/3, 0.25	1	0.38(3)	2.04
Ba2	4f	2/3, 1/3, 0.4441(1)	1	0.18(2)	2.41
Ba3	4e	1, 0, 0.3462(1)	1	0.18(2)	2.27
M1(Sn/Mn)	2a	1, 0, 0.5	0.86(1)/0.14	0.03(3)	4.16/2.76
M2(Mn/Sn)	4f	1/3, 2/3, 0.4078(1)	0.88(1)/0.12	0.07(4)	3.67/5.54
M3(Mn)	4f	1/3, 2/3, 0.3013(1)	1	0.04(3)	3.98
O1	6h	0.1837(1), 0.8163(1), 0.25	1	0.08(2)	
O2	12k	0.1689(1), 0.3377(2), 0.4504(1)	1	0.43(1)	
O3	12k	0.4810(1), 0.9621(2), 0.3526(1)	1	0.26(3)	

Space group: $P6_3/mmc$; lattice parameter: $a = 5.717$ Å and $c = 23.534$ Å.

Table 2
Selected bond length of $Ba_5Sn_{1.1}Mn_{3.9}O_{15}$.

Bond length (Å)		
Ba1–O1(×6) 2.865(1)	Ba3–O1(×3) 2.905(1)	Mn1/Sn–O3(×3) 1.959(1)
Ba1–O3(×6) 3.037(1)	Ba3–O2(×3) 2.969(1)	Mn2–O1(×3) 1.914(1)
Ba2–O2(×6) 2.864(1)	Ba3–O3(×6) 2.870(1)	Mn2–O3(×3) 1.897(1)
Ba2–O2(×3) 2.972(1)	Sn/Mn–O2(×6) 2.040(1)	Mn1–Mn2 2.509(2)
Ba2–O3(×3) 2.832(1)	Mn1/Sn–O2(×3) 1.912(1)	Mn2–Mn2 2.419(3)

The R_{wp} and χ^2 parameters are 5.8% and 3.9 for the refinement, respectively.

The refined atomic parameters and bond distances are listed in Tables 1 and 2, respectively. M1 site is dominated by Sn atom (occupancy 86%) and M2 site is dominated by Mn atom (occupancy 88%). The BVS calculation reveals that Mn atom displays a relatively low valence (2.76 at M1 site and 3.67 at M2 site) and Sn atom displays a relatively high valence (4.16 at M1 site and 5.54 at M2 site). This agrees with the disordered model well. Different atoms in the same crystallographic site have different local coordination, but an average set of coordination was used in the structural refinement. As a result, the larger ions show relative higher valences and the smaller ones show relative lower valences. Mn atoms at M3 site show 4+ valences, indicating no disorder occurs.

It is interesting to notice that the distortions of MnO_6 octahedra in the face-sharing octahedral chain. The Mn atoms at M2 site deviate from the octahedral centre: the bond length of Mn_{M2}–O2 and Mn_{M2}–O3 are 1.912 and 1.959 Å, respectively. The Mn atoms at M3 site also deviate from the octahedral centre: Mn_{M3}–O1 and Mn_{M3}–O3 are 1.914 and 1.897 Å, respectively. As a result, two different sets of Mn–Mn distance are got: Mn_{M2}–Mn_{M3} is 2.509 Å and Mn_{M3}–Mn_{M3} is 2.419 Å. Because of this distortion, both Mn–Mn distances become larger than the one (2.407 Å) in 2H $BaMnO_3$ [3], which help to stabilize the 10H perovskite structure.

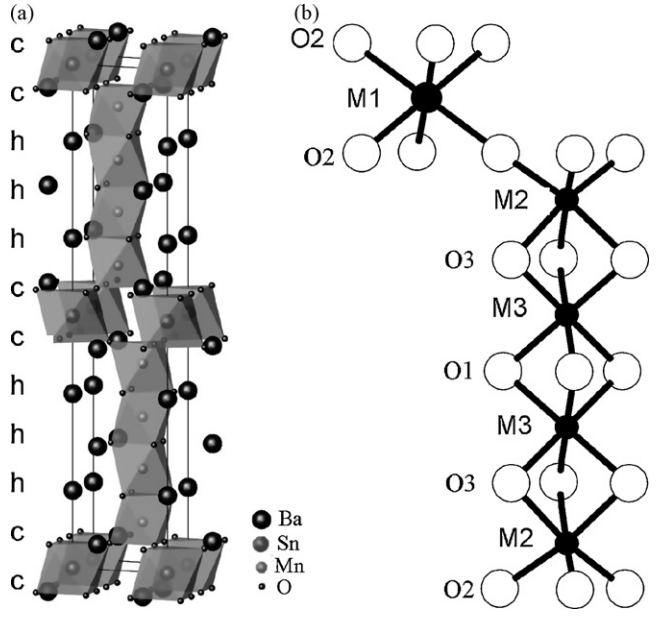

Fig. 4. Schematic representations of (a) the structure and (b) the polyhedra sites corresponding to $Ba_5Sn_{1.1}Mn_{3.9}O_{15}$. Three different metal sites are marked as M1, M2, M3 in plot (b).

The crystal structure of $Ba_5Sn_{1.1}Mn_{3.9}O_{15}$ is shown in Fig. 4. $Ba_5Sn_{1.1}Mn_{3.9}O_{15}$ can be described with 10H hexagonal perovskite, in which close packing BaO_3 layers stack following a sequence $(cchhh)_2$ and octahedral sites M1, M2 and M3 are formed between BaO_3 layers. The face-sharing and corner-sharing octahedral sites are mainly for Mn and Sn atoms, respectively. Although M1 and M2 are co-occupied by Sn and Mn atoms, the local structure is dominated by the octahedral chains Mn_4O_{15} and octahedral SnO_6.

But in 10H $Ba_5In_{0.94}Mn_4O_{14.40}$ structure, Mn atoms occupy M2 and M3 site exclusively, and In atoms occupy M1 site exclusively. The structural difference comes from the ionic radius and charge differences of dopant elements. The ionic radius of 6-coordinated In^{3+}, Sn^{4+} and Mn^{4+} is 0.8, 0.69 and 0.53 Å, respectively [27]. Sn^{4+} is closer to Mn^{4+} in size than In^{3+}. Furthermore, Sn^{4+} ion has the same valence with Mn^{4+} ion. As a result, some amount of disorder occurs between Sn^{4+} and Mn^{4+}, resulting in narrow solid solution and non-stoichiometric Sn/Mn ratios.

3.2. Magnetization

Temperature dependent DC magnetic susceptibility is shown in Fig. 5. The susceptibility changes little in 100–300 K and starts to increase smoothly as temperature goes down. This indicates the sample is a paramagnetic insulator with anti-ferromagnetic interaction between magnetic moments above 100 K. A slop change of the magnetic susceptibility is observed at about 7 K (shown in Fig 5a), below which ZFC and FC magnetic susceptibility starts to diverge (shown in Fig. 5b). In addition, the AC magnetic susceptibility χ' shows a peak at about 7 K, which is slightly frequency-dependent as shown in Fig. 6. This suggests the magnetic transition at 7 K is a spin glass transition [28]. Small loop observed in M–H curve measured at 2 K agrees with such behavior. A second peak observed at about 36 K in AC magnetic susceptibility, is due to small amount of Mn_3O_4 impurity, as observed by Attfield in Mn_2OBO_3 system [29], which is confirmed by the 10 K neutron pattern with a magnetic peak [1 1 0] of Mn_3O_4 (T_F 42 K) at $d = 4.9$ Å as shown in Fig. 7. The 10 K neutron diffraction data can be well-fitted with atomic structure only, which suggest no long range order magnetic phase transition.

Such magnetic behavior keeps with the crystal structure. In In/Sn-doped $BaMnO_3$, as the dopant have no magnetic moment, the difference of the magnetic properties are due to the different arrangements of Mn atoms in these two compounds. In $Ba_5Sn_{1.1}Mn_{3.9}O_{15}$, the arrangements of Mn atoms are very com-

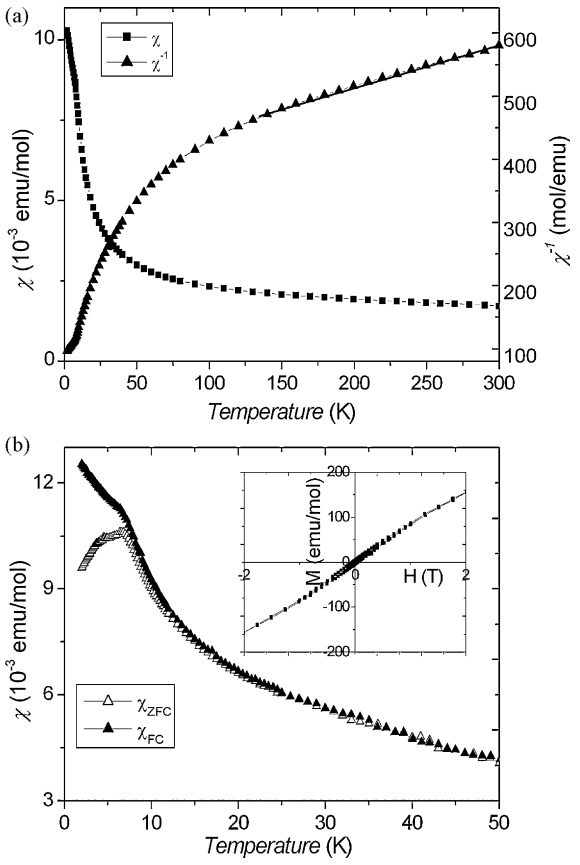

Fig. 5. (a) Magnetic susceptibility and inverse magnetic susceptibility of $Ba_5Sn_{1.1}Mn_{3.9}O_{15}$ measured at 1000 Oe, (b) magnetic susceptibility under zero filed cooling and field cooling (20 Oe) between 2 and 50 K, and the field dependence of magnetization at 2 K (inset) of $Ba_5Sn_{1.1}Mn_{3.9}O_{15}$.

plex. Three kinds of face-sharing octahedral chains Mn_4O_{15} (77%), $SnMn_3O_{15}$ (21%), and $Sn_2Mn_2O_{15}$ (2%) form in $Ba_5Sn_{1.1}Mn_{3.9}O_{15}$, but $SnMn_3O_{15}$ and $Sn_2Mn_2O_{15}$ block long range inter-chain interactions. The face-sharing octahedral chains are connected with SnO_6 (86%) or MnO_6 (14%) octahedra via corners. The dominating structure is Mn_4O_{15} octahedral chains connected with SnO_6 octahedra, which is similar to $Ba_5In_{0.93}Mn_4O_{14.40}$ and results a similar paramagnetic behavior above 100 K for both compounds. Long range inter-chain interactions occur only when the face-sharing octahedral chains Mn_4O_{15} are connected with MnO_6 octahedra, which are the rare case (1% per unit cell), thus long range

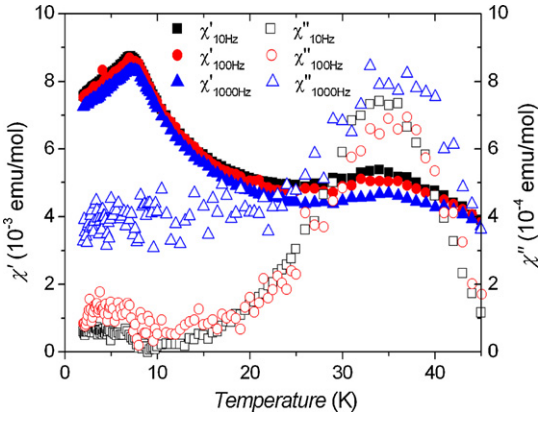

Fig. 6. Temperature dependent AC magnetic susceptibility of $Ba_5Sn_{1.1}Mn_{3.9}O_{15}$ measured in the applied filed of H_{DC} = 0 Oe and H_{AC} = 3 Oe at different frequencies.

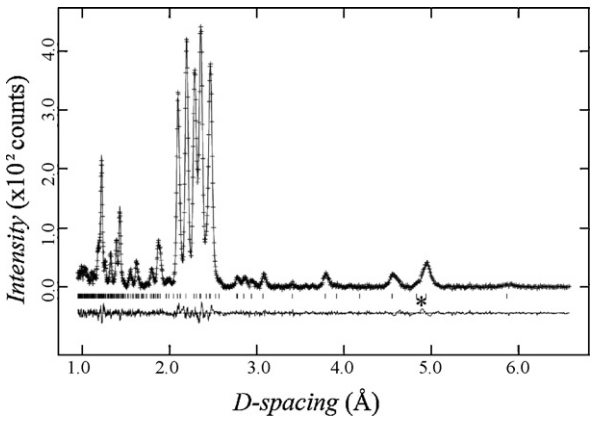

Fig. 7. Observed, calculated, and differential neutron diffraction pattern collected at 10 K of $Ba_5Sn_{1.1}Mn_{3.9}O_{15}$. Mn_3O_4 impurity peak is marked with asterisk.

order is prohibited, and spin glass behavior is observed at about 7 K.

4. Conclusions

A new barium tin manganese oxide $Ba_5Sn_{1.1}Mn_{3.9}O_{15}$ has been synthesized at 1300 °C in air by traditional solid-state reaction. It is a 10H hexagonal perovskite compound. The closed-packed $[BaO_3]$ layers stack in the $(cchhh)_2$ sequences, Mn and Sn atoms occupy M1, M2 and M3 sites in a partial ordered way. The face-sharing octahedral sites M2 and M3 are mainly occupied by Mn atoms and the corner-sharing octahedral site M1 is dominated by Sn atoms. The difference between 10H-$Ba_5In_{0.93}Mn_4O_{14.40}$ and $Ba_5Sn_{1.1}Mn_{3.9}O_{15}$ comes from the different charge and radius of the dopant ions.

Although the occupancy of the dopant and Mn atom show some differences, the magnetic properties are quite similar for $Ba_5In_{0.93}Mn_4O_{14.40}$ and $Ba_5Sn_{1.1}Mn_{3.9}O_{15}$, showing strong antiferromagnetic interactions above 100 K. However, spin glass behavior was observed at 7 K for $Ba_5Sn_{1.1}Mn_{3.9}O_{15}$.

Acknowledgments

This work is supported by the National Natural Science Foundation of China (Grant 20771008). The authors thank Prof. J. Paul Attfield for the fruitful discussions.

References

[1] J.M. Gonzalez-Calbet, M. Parras, J.M. Alonso, M. Vallet-Regi, J. Solid State Chem. 106 (1993) 99–110.
[2] T. Negas, R.S. Roth, J. Solid State Chem. 3 (1971) 323–339.
[3] E.J. Cussen, P.D. Battle, Chem. Mater. 12 (2000) 831–838.
[4] J.J. Adkin, M.A. Hayward, Chem. Mater. 19 (2007) 755–762.
[5] J.J. Adkin, M.A. Hayward, J. Solid State Chem. 179 (2006) 70–76.
[6] A. Querejeta, A. Varela, M. Parras, F. del Monte, M. Garcia-Hernandez, J.M. Gonzalez-Calbet, Chem. Mater. 21 (2009) 1898–1905.
[7] J. Hadermann, A.M. Abakumov, J.J. Adkin, M.A. Hayward, J. Am. Chem. Soc. 131 (2009) 10598–10604.
[8] J.J. Adkin, M.A. Hayward, Inorg. Chem. 47 (2008) 10959–10964.
[9] G.M. Keith, C.A. Kirk, K. Sarma, N.M. Alford, E.J. Cussen, M.J. Rosseinsky, D.C. Sinclair, Chem. Mater. 16 (2004) 2007–2015.
[10] N. Floros, C. Michel, M. Hervieu, B. Raveau, J. Solid State Chem. 168 (2002) 11–17.
[11] N. Floros, C. Michel, M. Hervieu, B. Raveau, Chem. Mater. 12 (2000) 3197–3201.
[12] N.A. Jordan, P.D. Battle, J. Mater. Chem. 13 (2003) 2220–2226.
[13] H. Yang, Z.E. Cao, X. Shen, W.J. Feng, J.L. Jiang, J.F. Dai, R.C. Yu, J. Mater. Sci. 43 (2008) 5679–5684.
[14] H. Yang, Y.K. Tang, L.D. Yao, W. Zhang, Q.A. Li, F.Y. Li, C.Q. Jin, R.C. Yu, J. Alloys Compd. 432 (2007) 283–288.
[15] X.J. Kuang, C. Bridges, M. Allix, J.B. Claridge, H. Hughes, M.J. Rosseinsky, Chem. Mater. 18 (2006) 5130–5136.
[16] A.F. Fuentes, K. Boulahya, U. Amador, J. Solid State Chem. 177 (2004) 714–720.
[17] C. Rabbow, H. Mullerbuschbaum, Z. Naturforsch. (B) 49 (1994) 1277–1281.

[18] C.L. Yin, G.B. Li, T.N. Jin, L.P. You, J.L. Tao, J.W. Richardson, C.K. Loong, J.L. Sun, F.H. Liao, J.H. Lin, Chem. Mater. 20 (2008) 2110–2116.
[19] N. Creon, C. Michel, A. Hervieu, A. Maignan, B. Raveau, Solid State Sci. 5 (2003) 243–248.
[20] L. Miranda, A. Feteira, D.C. Sinclair, M.G. Hernandez, K. Boulahya, M. Hernando, A. Varela, J.M. Gonzalez-Calbet, M. Parras, Chem. Mater. 20 (2008) 2818–2828.
[21] L. Miranda, J. Ramirez-Castellanos, A. Varela, J.M. Gonzalez-Calbet, M. Parras, M. Hernando, M.T. Fernandez-Diaz, M.G. Hernandez, Chem. Mater. 19 (2007) 1503–1508.
[22] J.G. Zhao, L.X. Yang, Y. Yu, F.Y. Li, R.C. Yu, C.Q. Jin, J. Solid State Chem. 181 (2008) 1767–1775.
[23] L. Miranda, J. Ramirez-Castellanos, M. Hernando, A. Varela, J.M. Gonzalez-Calbet, M. Parras, Eur. J. Inorg. Chem. 15 (2007) 2129–2135.
[24] A.C. Larson, R.B. Von Dreele, General Structure Analysis System (GSAS), Los Alamos National Laboratory Report LAUR Los Alamos, 2004, pp. 86–748.
[25] C. Dong, J. Appl. Crystallogr. 32 (1999) 838.
[26] A. Altomare, M.C. Burla, M. Camalli, G.L. Cascarano, C. Giacovazzo, A. Guagliardi, A.G.G. Moliterni, G. Polidori, R. Spagna, J. Appl. Crystallogr. 32 (1999) 115–119.
[27] R.D. Shannon, Acta Cryst. A32 (1976) 751–767.
[28] C.A.M. Mulder, A.J. van Duyneveldt, J.A. Mydosh, Phys. Rev. B 23 (1981) 1384–1396.
[29] R.J. Goff, A.J. Williams, J.P. Attfield, Phys. Rev. B 70 (2004) 014426.